Organic & Biomolecular Chemistry

RSC Publishing

PAPER

View Article Online
View Journal | View Issue

Cite this: *Org. Biomol. Chem.*, 2013, **11**, 640

Structural characterization of a peptoid with lysine-like side chains and biological activity using NMR and computational methods†

Ulrich Sternberg,[a] Esther Birtalan,[b] Igor Jakovkin,[a] Burkhard Luy,[a,b] Ute Schepers,[c] Stefan Bräse*[b] and Claudia Muhle-Goll*[b]

Received 26th July 2012,
Accepted 23rd November 2012

DOI: 10.1039/c2ob27039k

www.rsc.org/obc

N-Substituted glycine oligomers or peptoids with charged side chains are a novel class of cell penetrating peptide mimetics and have been shown to serve as drug delivery agents. Here, we investigated by NMR spectroscopy and quantum chemical calculations whether a Rhodamine B labelled peptoid [RhoB^{Spiro}-Ahx]-[But]$_{6A}$NH$_2$ with lysine-like side chains adopts structural motifs similar to regular peptides. Due to a low chemical shift dispersion, high resolution structure determination with conventional NMR-derived distance restraints and *J*-couplings was not possible. Instead, a combined assignment and structure refinement strategy using the QM/MM force field COSMOS-NMR was developed to interpret the highly ambiguous chemical shift and distance constraints and obtain a medium resolution three-dimensional structural model. This allowed us to select for the all *cis*-amide conformation of the peptide with a pseudo-helical arrangement of extended side chains as a faithful representative structure of [RhoB^{Spiro}-Ahx]-[But]$_{6A}$NH$_2$. We tested the biological activity of the peptoid by live-cell imaging, which showed that the cellular uptake of the peptoid was comparable to conventional cell-penetrating peptides.

Introduction

Cell penetrating peptides (CPPs) consisting of 10–30 mainly cationic and hydrophobic amino acids are frequently used for medicinal purposes. Due to their amphiphilic polycationic nature they display good cell penetrating abilities. It was shown that they could carry cargos such as oligonucleotides,[1] liposomes,[2] and nanoparticles into cells.[3] The fast cellular uptake and the well-defined chemistry make CPPs very attractive for potential pharmaceutical applications,[4–7] and they are increasingly discussed for use in targeted drug delivery due to their higher proteolytic stability.

Currently, peptidomimetics of these CPPs are under investigation for a wide range of biological applications. In contrast to peptides, they are usually stable against proteases and therefore represent promising drug candidates. One class of these CPP mimetics is the so called cell penetrating peptoids (CPPos). Peptoids are oligo-*N*-substituted glycines in which side chains are shifted from the α-carbon to the nitrogen atom. This difference in conformation has profound consequences on the structure of the peptoids, because they are not able to form backbone hydrogen bonds, which in peptides lead to well-known secondary structural motifs like α-helices or β-sheets.[8]

Nevertheless, several efforts to induce secondary structural motifs into peptoids were successful. Likewise, it turns out that backbone structural preferences in peptoids can be governed by local interactions, including steric, stereoelectronic and bond-resonance effects. Efforts to induce secondary structural motifs into peptoids comprised the introduction of branching, bulky substituents to enhance a steric repulsion between side chains,[9,10] as well as negatively charged side chains, which cause electrostatic repulsion with backbone carbonyls.[11] Hydrophobic interactions[12] and n→p* interactions between side chains have also been predicted to play a role in peptoid folding.[13]

Systematic comparison of peptides and peptoids by theoretical calculations at various levels of approximation (*ab initio*

[a]*Karlsruhe Institute of Technology (KIT), Institute for Biological Interfaces, POB 3640, D-76021 Karlsruhe, Germany*
[b]*Karlsruhe Institute of Technology (KIT), Institute of Organic Chemistry, Fritz-Haber-Weg 6, D-76131 Karlsruhe, Germany. E-mail: claudia.muhle@kit.edu, braese@kit.edu; Tel: (+49) 721 608-45344, (+49) 721 608-42902*
[c]*Karlsruhe Institute of Technology (KIT), Institute of Toxicology and Genetics, POB 3640, D-76021 Karlsruhe, Germany*

†Electronic supplementary information (ESI) available: Table S1: NOE data, Table S2: calculated and experimental ^{13}C CS for the best *cis* and *trans* peptoid structure, Table S3: calculated and experimental ^{13}C CS of Rhodamine B in D$_2$O, Table S4: summary of the structure investigation, Fig. S1 and S2: chemical structure and nomenclature of [RhoBSpiro Ahx] [BUT]$_{6A}$NH$_2$ and Rhodamine B. See DOI: 10.1039/c2ob27039k

and semi-empirical MO (molecular orbital) theory, molecular mechanics) yielded models of their basic structural units and their distinct conformational differences.[14,15] In recent years, the two- or three-dimensional structures of various peptoids were elucidated: in solution by circular dichroism and NMR spectroscopy, and in solids by X-ray crystallography (*e.g.* ref. 10, 16–18). In peptoids, both *cis* and *trans* conformations can be detected similar to what is observed for prolines.[19] The amide nitrogen substituent dictates the geometry of the amide bond. Peptoids with α-chiral, bulky side chains have been found to preferentially form *cis*-amide bonds.[20,21] *N*-Aryl-substituted peptoids adopted mainly *trans*-amide conformations due to steric and electronic preferences. Peptoids containing *N*-hydroxy-amides were recently shown to form sheet-like structures with *trans*-amide bonds.[22]

The side chains employed in the above-mentioned structural studies were chemically quite different from those of natural amino acids. Structures of peptoids and peptomers with amino acid-like side chains attached to the nitrogen atom and biological membrane activity have so far only been simulated to our knowledge.[23]

Wender and coworkers showed that side chain groups like guanidino or amino groups play an important role in facilitating cellular uptake of HIV Tat-derived CPPs whereas charge or backbone conformations seemed to be of minor importance for peptide import.[6] However, CPPos with side chains consisting of a guanidine group at the end of a six-methylene group spacer were more potent cell transporters than their related peptides.

We recently published the synthesis of a Rhodamine B labelled CPPo containing six lysine-like side chains (Fig. 1).[24] The attached Rhodamine B fluorophore facilitates tracking within living cells and allows for the study of their interaction with membranes and cell organelles. We show here that this CPPo is biologically active and accumulates in endosomes, and that it adopts an extended pseudo-helical conformation with predominantly *cis*-amide bonds *in vitro*.

To solve the structure of the peptoid a combination of nuclear magnetic resonance (NMR) spectroscopy and constrained molecular mechanics was used. Chemical shifts computed *via* Bond Polarization Theory (BPT)[25] were used as the main source of structural constraints to select the correct structural model, which corresponds to the all *cis*-amide conformation.

To our knowledge, chemical shift (CS) driven geometry optimization was applied for the first time to calculate the structure of a cyclic pseudo-peptide that forms a zinc complex.[26] Here, we show that this method can be employed in a case where conventional structure determination based on *J*-couplings and NOE-derived distances is bound to fail due to heavy chemical shift overlap.

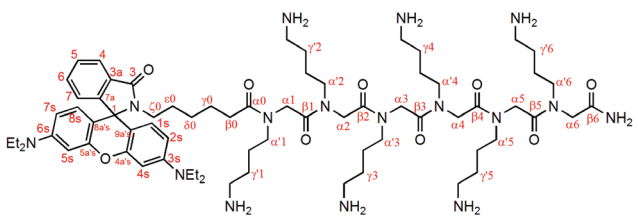

Fig. 1 Structure of the Rhodamine B-labelled oligo-*N*-substituted glycine [RhoB^{Spiro}-Ahx]-[But]$_{6A}$NH$_2$.

Results and discussion

Biological activity

Most of the CPPos containing lysine or similar side chains with a terminal amino group at the nitrogen atom accumulate in endosomes after endocytosis and are eventually released into the cytosol, depending on the ratio of their positive charges and the hydrophobicity of the side chains. CPPos containing more lipophilic side chains have been shown to be targeted instead to mitochondria. The structural requirements for endosomal accumulation or endosomal export still remain unknown.

We tested the cellular uptake of [RhoB^{Spiro}-Ahx]-[But]$_{6A}$NH$_2$ in HeLa cells (Fig. 2). To visualize the cellular uptake, the endosomal accumulation, and a possible endosomal escape, HeLa-cells were incubated with 1 μM [RhoB^{Spiro}-Ahx]-[But]$_{6A}$NH$_2$ for 12 hours. After a few minutes [RhoB^{Spiro}-Ahx]-[But]$_{6A}$NH$_2$ was taken up by endocytosis and accumulated in the endosomal compartments in the perinuclear region (Fig. 2B).

After longer exposure of the cells with higher concentrations of the peptide a staining of nucleoli was observed (data not shown).

Relation to structure

Electrostatic interactions play a significant role in the membrane affinity of cationic moieties. With a pK_a of 10.4, the side chains of [RhoB^{Spiro}-Ahx]-[But]$_{6A}$NH$_2$ display a similar pK_a as lysine. In aqueous solution the peptoid will be highly charged under biological conditions as the amino groups are protonated and transform into $(NH_3)^+$-groups, resulting in a total charge of the molecule of +6. These charged groups can strongly interact with the negatively charged proteoglycans at the plasma membrane attracting the [RhoB^{Spiro}-Ahx]-[But]$_{6A}$NH$_2$ close to the lipid bilayer. This leads to an accumulation on the cell membrane surface, where the peptoid waits for endocytosis. The charged groups of [RhoB^{Spiro}-Ahx]-[But]$_{6A}$NH$_2$ can strongly interact with charged lipids of the

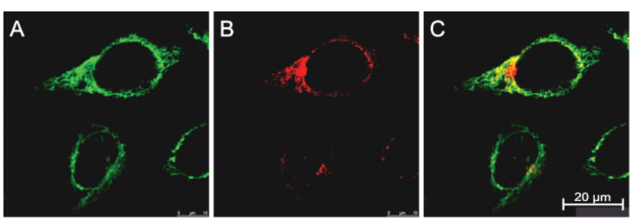

Fig. 2 Immunofluorescence analysis of HeLa-cells incubated with 1 μM [RhoB^{Spiro}-Ahx]-[But]$_{6A}$NH$_2$ for 12 hours at 37 °C. Staining with (A) MitoTracker, (B) [RhoB^{Spiro}-Ahx]-[But]$_{6A}$NH$_2$. (C) Merge. Endosomes appear to be the main targets of [RhoB^{Spiro}-Ahx]-[But]$_{6A}$NH$_2$.

endosomal/lysosomal compartment such as zwitterionic lipids and the negatively charged phospholipids leading to accumulation and partitioning of the endosomal membrane. It has been shown that cell cationic amphiphiles with membrane affinity can have varying effects on phospholipid vesicles by disordering the lipid bilayer, depending on how the structure of the molecule intercalates into the lipid bilayer. In analogy to CPPs, depending on their fold, CPPos are sufficiently bulky to create steric disruption: being involved in the lipid interfacial/headgroup electrostatic interaction, disrupting the lipid packing leads to a higher mobility of the acyl chains, which eventually catalyses the formation of membrane pores at higher CPPo concentrations. At low CPPo concentration these pores are only transient allowing the CPPo to slip through the membrane.

Many cell penetrating peptides have been reported to be structurally flexible ranging from no specific (random coil) structures in aqueous solutions to α-helical, β-sheet or β-turn structures upon interaction with lipid membranes (*e.g.* ref. 27–29). Proline-rich CPPs with proline contents up to 50% typically adopt poly-proline II pseudohelical structures already in aqueous buffers in the absence of lipid membranes.[30] Although details of the membrane passage are not known, it is commonly believed that the observed structuring can be a prerequisite to pass the membrane. In analogy to CPPs it is conceivable that CPPos are also structured upon interaction with the membrane, which would be in line with the observation that several peptoids have been shown to adopt a pseudohelical conformation.[10,16,19] However, the corresponding structures have been mainly determined in organic solvents, which provide an environment that differs considerably from aqueous solutions in its physicochemical properties. Thus, in order to get a defined view of the peptide before its interaction with a membrane, we aimed to solve the structure of the biologically active [RhoB^{Spiro}-Ahx]-[But]$_{6A}$NH$_2$ in water.

NMR-spectroscopy

To derive the three-dimensional structure of [RhoB^{Spiro}-Ahx]-[But]$_{6A}$NH$_2$ in solution we recorded a set of 2D-^{1}H-NMR spectra in H_2O and D_2O. Since [RhoB^{Spiro}-Ahx]-[But]$_{6A}$NH$_2$ has no amide hydrogen atoms and all side chains of [RhoB^{Spiro}-Ahx]-[But]$_{6A}$NH$_2$ are chemically identical, hydrogen and carbon signals from different side chains largely overlapped (Fig. 3A). 2D TOCSY, NOESY or ROESY, and ^{1}H, ^{13}C-HSQC spectra allowed the classification of resonances to atom groups within residues (*e.g.* H_α and C_α resonances could be distinguished from those of $H_{\alpha'}$ and $C_{\alpha'}$), but it was not possible to sequentially assign the resonances. Several strong ROEs in ROESY spectra of 70 and 200 ms mixing time could be identified which connect H'_α resonances with H_α, whereas only a few weak ROEs between vicinal H_α resonances were detectable (Fig. 3B). Such a pattern is consistent with a *cis*-amide conformation.[19] The chemical shift range for the $^{13}C_\alpha$ carbons also agrees well with values previously reported by Kirshenbaum and coworkers for a peptoid *cis* conformation.[10] NOE-derived distance restraints alone, however, did not allow the construction of a 3D structural model due to the unsolved chemical shift ambiguities. Thus, we decided to use the CS values as additional restraints for structure calculation using the COSMOS-NMR force field.

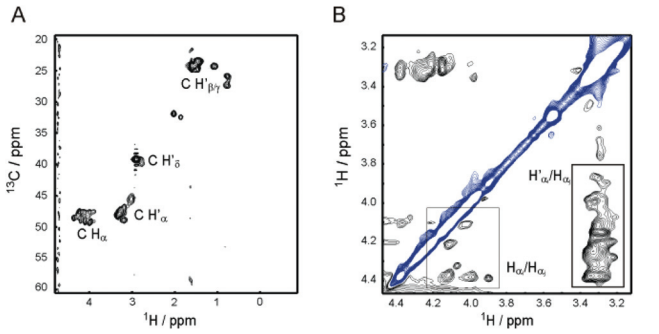

Fig. 3 (A) ^{1}H-^{13}C-HSQC spectrum of [RhoB^{Spiro}-Ahx]-[But]$_{6A}$NH$_2$ in 90% H_2O/10% D_2O. Resonances of functional groups are labelled. (B) Partial view of a 2D ROESY spectrum showing ROEs between H_α and $H_{\alpha'}$.

Structure modeling

Several groups have developed computational methods that use chemical shifts as a source for protein structure calculation, relying on empirical CS databases.[31–33] However, a comparable data base does not exist for peptoids. Thus, we computed the chemical shifts using the BPT approach.[25,34] The BPT is a semi-empirical method for the calculation of localised molecular properties such as partial atomic charges, chemical shifts and *J*-couplings. It is implemented in the QM/MM (quantum mechanics/molecular mechanics) COSMOS-NMR force field,[35] which can be applied to the vast majority of organic molecules (and even several types of metal complexes) without the need of specialised force field parameterizations for each substance class. For every bond defined within the force field bond orbitals are constructed from Slater type atomic orbitals. The molecular properties are calculated within the BPT framework from perturbation expressions of these bond orbitals. This procedure leads to a special QM/MM force field where the electrostatic interactions including all polarizations are calculated from BPT partial charges instead of using fixed atom charges as defined in common force fields. To calculate the partial charge of an atom all other atomic charges of the molecular system need to be known. This leads to a set of equations corresponding to the number of atoms in the system under investigation, where all charges in the molecule are simultaneously determined.[36] The parametrization of the perturbation expression has been performed using *ab initio* TZVPP-MP2 calculations[25] on small molecules.

The BPT atomic charges can be calculated at every step of molecular mechanics calculations making the force field generally more applicable to different substances and more flexible. Moreover the number of semi-empirical BPT parameters is much smaller than the types of fixed atomic charge parameters of traditional force fields. The treatment of all mutual polarization on the quantum-chemical BPT level makes

COSMOS-NMR even applicable for highly charged molecules and ions.

The perturbation equations for bond orbitals can also be parametrized to allow the calculation of chemical shifts, which can be regarded as mainly localized properties. The chemical shifts can be split up into individual orbital contributions.[37] Since large contributions to the chemical shift arise from bonds near the nucleus of interest, in the BPT framework the chemical shift of an atom is the sum of individual bond contributions of the bonds connected to the atom. If delocalization is neglected, even the influence of polarization of the bonds on the chemical shift can be split up into bond contributions.

Analogous to the atomic charges the chemical shifts are parametrized on *ab initio* calculations on a larger number of small molecules. With these calculated chemical shifts the two BPT parameters per bond type can be determined from a set of linear equations.[38] For a more comprehensive explanation of BPT and COSMOS-NMR we refer to ref. 35 and 38.

Since so far little NMR data (CS or characteristic NOEs) of peptoids are available, we built two starting models, one with all *cis*-amide and one with all *trans*-amide conformations to account for the possibility that peptoids can display both geometries. All lysine like amino groups were protonated and regarded as positively charged. After geometry optimization, the two peptoid models were subjected to an initial 1 ns molecular dynamics (MD) simulation at 500 K using the QM/MM COSMOS-NMR force field. Five hundred structures (MD snapshots) were stored for each peptoid conformation to generate a library of possible structures. After a subsequent round of geometry optimization, ^{13}C CSs were calculated on the BPT level for each of the 1000 structures. The best fit to the calculated BPT values was used as a criterion to assign ambiguous CS values for the 1000 structures. An additional requirement was that each CS value should be assigned and used at least once. The NOE derived distances were classified as strong ($H_{\alpha'}/H_{\alpha}$, 2.5 Å ± 1 Å) and weak ($H_{\alpha'}/H_{\alpha'}$, 4.5 Å ± 1 Å) (ESI Table S1†) and were assigned with the prerequisite that a trivial assignment to geminal protons on the same glycine analogue carbon was excluded. The automated assignment process stored every NOE constraint that fitted to a combination of sites within a cutoff value of ±1.0 Å.

In a second step, structure refinement was performed for all 1000 initial structural models using experimental data as constraints (60 automatically assigned CSs and 80 (*cis*) and 68 (*trans*) NOEs) including now pseudo-forces for chemical shifts and NOE-derived distances. In this geometry optimization the atomic charges of all atoms and the ^{13}C CS of the 60 sites were recalculated after every refinement step. The resulting conformers with lowest energies can be viewed as medium resolution models of the best structure of the peptoid in Fig. 5. In the following, individual structural features are discussed in detail.

Cis vs. trans conformation

After sorting of the final structures according to their pseudo-energies a clear preference for the *cis*-amide conformation was observed in accordance with our initial assumptions from the experimental data. The best 144 structures in terms of pseudo-energy displayed an all *cis*-amide conformation (Fig. 4A and B). A closer look at individual energy contributions revealed that the CS pseudo-energies yielded the decisive criterion to

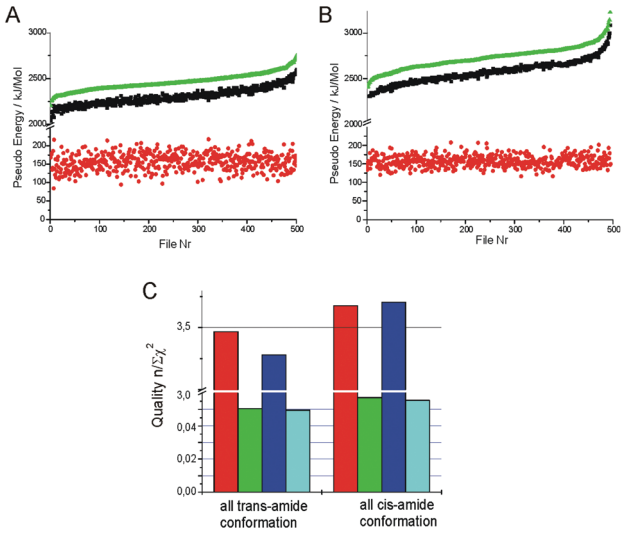

Fig. 4 (A, B) Pseudoenergies calculated for the 500 structures of (A) the all *cis*-amide conformation and (B) the all *trans*-amide conformation. Red: distance contribution to the pseudoenergy, green: BPT/CS contribution, black: total pseudo-energy. (C) Quality indicators for structure refinement of the two peptoid amide backbone conformations. The two leftmost columns show the quality values for the very best structure of each conformation (NOE distance: red, CS values: green) while the other two columns show corresponding values calculated for the 10 best structures (NOE distance: blue, CS values: light blue).

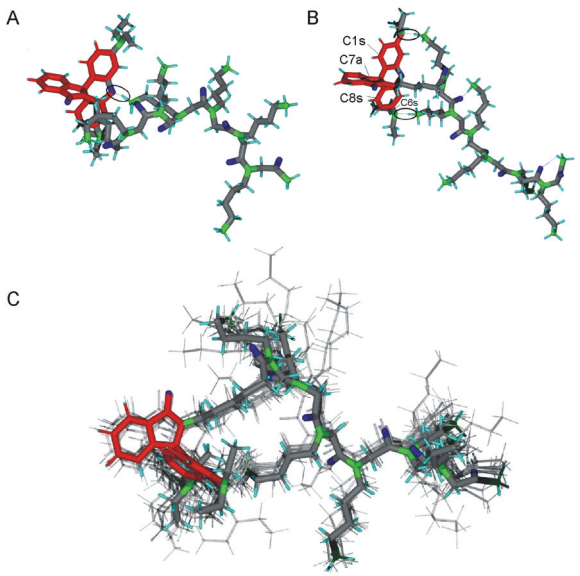

Fig. 5 The *cis* form (A) and the *trans* form (B) of the peptoid. The hydrogen bridges of side chains to the Rhodamine are indicated by ellipsoids. In (B) Rhodamine sites with CS differences to the experiment larger than 4 ppm are indicated. (C) Structure assemble of [$RhoB^{Spiro}$-Ahx]-[But]$_{6A}NH_2$ as obtained by a QM/MM refinement using the COSMOS-NMR force field. The 10 best structures were selected from a library of 500 models (the Rhodamine group is shown in red).

distinguish between the two conformations. Although the observed NOEs between Gly $H_\alpha(i)$/Gly $H_\alpha(i+1)$ have been reported as characteristic for *cis*-conformations,[19] the necessary high distance error bounds due to heavy overlap and missing chemical shift assignment led to similar NOE pseudo-energies for both conformers. Correspondingly, the distance root mean square deviations (RMSD) for both forms were similar, 0.52 Å for the *cis* form and 0.54 Å for the *trans* form. A table summarizing the statistics is given in ESI Table S4.†

Whereas deviations between experimental and calculated CS of the α′, β′, and γ′ side chain carbons were comparably high for both forms, the backbone carbons displayed deviations mostly below 2 ppm (ESI Table S2†), but the difference between the two peptoid conformations was not very pronounced. A reason for this is that the CSs of the peptoid backbone are influenced by a multitude of different conformations of the lysine-like side chains, and this dynamics obviously blurs out most CS differences caused by the backbone structure. The Rhodamine part of the molecule, however, is rather stiff, and its environment is clearly distinct in the two conformations. In the *cis*-amide conformation the orientation of the Rhodamine group is controlled by a hydrogen bridge between the lysine like NH_3^+ group of residue 3 to an oxygen atom of Rhodamine (Fig. 5A). In the *trans*-amide conformation two hydrogen bonds of NH_3^+-side chains 1 and 2 are formed for the nitrogen atoms of the diethylamino groups of Rhodamine (Fig. 5B). This caused large chemical shift errors with respect to the experimental values (ESI Table S2†). To understand whether the CS of the Rhodamine part can be sufficiently well calculated with the BPT approach to serve as a distinction criterion between the two peptoid conformations, we also calculated the CS of free Rhodamine B (ESI Table S3†). Most computed resonances agreed well with experimental values with the exception of resonances of 9′ and 9a′ and 8′ and 8a′, respectively. Thus, it seems feasible that the *cis*-amide conformation fits best to the observed shifts. To account for the different numbers of assigned NOE distances for the two structures we used a quality criterion that is derived from a χ value:

$$\chi^2 = \sum_i^n \left(\frac{\mathrm{Exp}_i - \mathrm{Calc}_i}{\mathrm{Error}_i}\right)^2$$

For reliable calculations the quality $Q = n/\chi^2$ should be larger than one (n being the total number of experimental data). In the case of the chemical shifts we used the error limits that we have previously estimated for proteins: 2.5 ppm.[38] This value is higher than the precision of the experiment, since CS calculations involve not only influences from torsion angles but also from bond distances and other details. Moreover, since the NMR experiments in solution reflect the CS mean value of a multitude of co-existing conformers, the mean chemical shift cannot be exactly represented by a single structure. As we can see from Fig. 4C, quality values for the *cis* conformation are higher.

After geometry optimization with CS as a target function, an RMS deviation of 3.33 ppm (3.36 ppm over all 10 best structures, the spiro carbon C1 and the ethyl carbons were excluded as their prediction is considered as being less reliable) was reached between the calculated and experimental chemical ^{13}C shifts (experimentally assigned CS values and their corresponding calculated values for the lowest pseudo-energy structure are given in ESI Table S2†) for the *cis* conformation. The best *trans* structures yielded a CS RMS deviation of 3.55 ppm leading to significantly higher pseudo-energies (Fig. 4A and B).

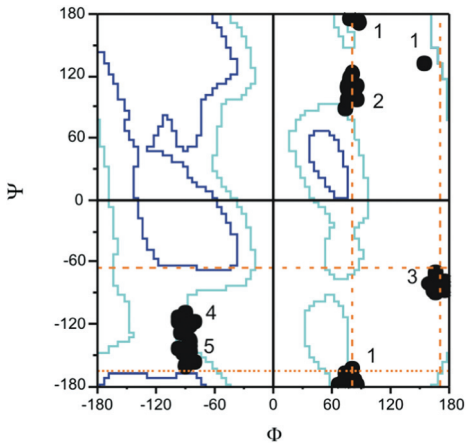

Fig. 6 Ramachandran plot of the structural ensemble of *cis* [RhoB^{Spiro}-Ahx]-[But]$_{6A}$NH$_2$. Filled cycles refer to ϕ, φ values for each residue in the 10 lowest energy conformations. The borders of most favourable regions for proteins are shown in blue; the borders of generally allowed regions are shown in cyan. Dashed lines indicate steric restrictions in proteins (black dashed line for O_{i-1}–C_β and orange dashed line for C_β–N_{i+1} steric clashes). Residues 5 and 6 lie in a favourable β-sheet region while residues 2 and 3 adopt peptoid specific extended geometries.

Structure description

We thus conclude that [RhoB^{Spiro}-Ahx]-[But]$_{6A}$NH$_2$ adopts preferentially the all *cis*-amide conformation in water. In this conformation, the peptoid has an extended pseudo-helical structure (Fig. 5C). Most of the backbones in the structural ensemble adopt backbone dihedral angles of ±(75°–95°) for Φ and ±100°–150° for Ψ (Fig. 6). The symmetry is clearly broken at Gly3 with a Φ value of ~170° and Ψ of ~−80°. This may be caused by an electrostatic interaction of the Lys4 side chain with Rhodamine, which is also reflected by a series of ROEs between the two groups. The Lys1 side chain forms a hydrogen bridge with a backbone carbonyl group.

Only the two backbone carbons of residues 4 and 5 display Φ, Ψ values commonly observed in proteins. The 3rd glycine analogue carbon displays extended β-sheet geometry with both Φ and Ψ angles clustering around 180°. Since the side chains are located at backbone *N*-sites, there is no strong repulsion between the backbone atoms and side chains. Moreover, secondary structure patterns in peptides and proteins are stabilized by formation of hydrogen bonds, which is ruled out in the peptoid. This leads to Φ, Ψ values that are excluded for L-amino acids, and can be regarded as peptoid-specific conformations.

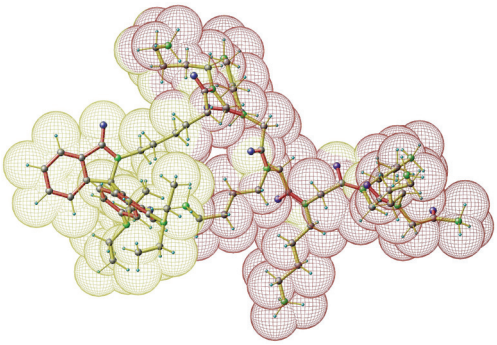

Fig. 7 Electrostatic potential at the surface of [RhoB^{Spiro}-Ahx]-[But]$_{6A}$NH$_2$. The plot is dominated by the positively (red) charged NH_3^+ groups. The nearly uncharged region around the Rhodamine is displayed in light yellow.

The hydrogen bridge between the Rhodamine ring and one lysine-like side chain stabilizes the position of the fluorophore.

The six charged side chains dominate the conformation of the molecule and their electrostatic repulsion tends to maximise the NH_3^+ distances (see Fig. 7). The interactions of charged side chains are sufficient to stabilize the extended pseudo-helical structure in the absence of hydrogen bonds. They provide an effective surface which resembles equivalent structures of multiple positively charged CPPs and corroborates their similar biological activity. The pitch of the pseudo-helix (7.7 ± 0.7 Å between C_β atoms of identically oriented side chains) differs from an α-helix and the charge distribution is less dense as compared to α-helical CPPs, potentially explaining small differences in the behaviour of the corresponding CPPos.

Conclusions

We have derived a medium resolution conformational model of [RhoB^{Spiro}-Ahx]-[But]$_{6A}$NH$_2$ by a novel approach, using NMR chemical shifts and sparse ambiguous distance restraints as the source of structural information in the QM/MM force field COSMOS-NMR. Using these data, a reasonable good agreement between experimental constraints and back-calculated CS values and distances was obtained. This indicates that the COSMOS-NMR derived models are a good representation of the [RhoB^{Spiro}-Ahx]-[But]$_{6A}$NH$_2$ average structure (Fig. 5). The data suggest that the 6-*mer* peptoid with lysine-like side chains adopts a pseudo-helical structure in water with an all-*cis*-amide conformation. Although it cannot be excluded that the conformation of [RhoB^{Spiro}-Ahx]-[But]$_{6A}$NH$_2$ changes upon contact with the membrane, a helical conformation together with positive charge has been found as a prerequisite for some CPPs to penetrate the membrane. Thus, [RhoB^{Spiro}-Ahx]-[But]$_{6A}$NH$_2$ seems to be a very good substitute for natural CPPs and indeed, we could demonstrate that [RhoB^{Spiro}-Ahx]-[But]$_{6A}$NH$_2$ shows membrane activity in HeLa cells and accumulates in endosomal/lysosomal compartments, which contain highly curved membrane structures.

Experimental section

The synthesis of [RhoB^{Spiro}-Ahx]-[But]$_{6A}$NH$_2$ has been recently published.[24]

Cell culture techniques for mammalian cells

Human cervix carcinoma cells (HeLa) were cultured under sterile conditions. 5 × 104 HeLa cells were plated into each well of an 8-well μslide from IBIDI (Ibitreat), Germany, and cultured in 200 μl of Dulbecco's modified Eagle's medium, high glucose (DMEM, Sigma Taufkirchen) supplemented with 10% fetal calf serum (FCS, PAA), and 1 μ ml^{-1} penicillin/streptomycin at 37 °C, 5% CO_2.

Treatment of adherent cells with [RhoB^{Spiro}-Ahx] [BUT]$_{6A}$NH$_2$

[RhoB^{Spiro}-Ahx] [BUT]$_{6A}$NH$_2$ was dissolved in bidistilled water to yield a 2 mM stock solution and was further diluted with 10% DMEM to yield the respective incubation media. The cells cultured as described above were incubated with [RhoB^{Spiro}-Ahx] [BUT]$_{6A}$NH$_2$ at final concentrations of 0.1, 1, 5, 10, 20, 50, and 100 μM, respectively. Cellular uptake of the peptoid was measured by live-cell imaging after 2, 4, and 16 h as fixation would alter the intracellular distribution as described for other polycationic species.

Subcellular localization

For the intracellular localization of the peptoids, the cells were co-incubated with fluorescent probes specific for different organelles (Molecular Probes, Karlsruhe). For mitochondria labeling the cells were treated with 100 nM Mitotracker®Green FM for 15 min, according to the manufacturer's manual, and washed three times with 1× PBS. The cells were covered with DMEM and subjected to live confocal microscopy at 37 °C and 5% CO_2 atmosphere.

Live imaging by confocal microscopy

Simultaneous visualization of the colocalization of [RhoB^{Spiro}-Ahx] [BUT]$_{6A}$NH$_2$ and cellular organelles was achieved by confocal microscopy using a Leica TCS-SP5 II, equipped with a DMI6000 microscope. For the colocalization with mitochondria, MitoTracker Green was excited using the 488 nm line of an argon ion laser, [RhoB^{Spiro}-Ahx] [BUT]$_{6A}$NH$_2$ was excited at 561 nm using a DPSS laser. The objective was an HCX PL APO lambda blue 20.0 × 0.70 IMM UV. The exposure was set to minimize oversaturated pixels in the final images. Fluorescence emission was measured at 503–538 nm (for Mitotracker®Green FM) and 580–653 nm (for [RhoB^{Spiro}-Ahx] [BUT]$_{6A}$NH$_2$) using the simultaneous detection of the Mitotracker®Green FM and the respective peptoid. Image acquisition was conducted at a lateral resolution of 1024 × 1024 pixels and 8 bit depth using LAS-AF 2.0.2.4647 acquisition software.

NMR spectroscopy

The peptoid was dissolved at a concentration of 8 mM in either 90% H_2O/10% D_2O or 100% D_2O. Two dimensional

^{1}H-^{1}H-TOCSY, ROESY, and NOESY spectra and two dimensional ^{1}H-^{1}H-^{13}C HMQC or HSQC spectra were recorded on a Bruker AVANCE 600 MHz spectrometer at 23 °C. Typical settings were 200 t_1 transients with 128 scans per transient for 2D-^{1}H-^{13}C spectra and 512 t_1 transients with 32 scans per transient for 2D-^{1}H spectra. Mixing times were 70 and 150 ms for ROESY spectra at a spin lock power of 4 kHz and 70, 100, 200 and 400 ms for NOESY spectra. Chemical shift values were referenced relative to an externally measured TMS sample. Spectra were analysed with TOPSPIN 3.0 (Bruker Biospin, Rheinstetten, Germany).

Molecular modelling and chemical shift calculation

Structure refinements were performed using the COSMOS-NMR force field (see *e.g.* ref. 35 and 39 and for the force field Möllhoff and Sternberg[34] and Sternberg *et al.*[25]). For the molecular modelling we used COSMOS Pro 5 providing a graphical user interface (GUI) for Windows. A backend version without the GUI, which runs on several operating systems including Unix and Linux, can be obtained from one of the authors (please contact U. Sternberg). Calculations for this paper were performed running the COSMOS-backend on the HP XC3000 (hc3) cluster of the KIT.

Acknowledgements

This work has been supported by the Center for Functional Nanostructures of the German Research Council (Projects E1.1) and a fellowship of the German Business Foundation (fellowship to E.B.). We also gratefully acknowledge the help of Dominik K. Kölmel during the synthesis of the molecule.

Notes and references

1 A. Astriab-Fisher, D. S. Sergueev, M. Fisher, B. R. Shaw and R. L. Juliano, *Biochem. Pharmacol.*, 2000, **60**, 83–90.
2 V. P. Torchilin, R. Rammohan, V. Weissig and T. S. Levchenko, *Proc. Natl. Acad. Sci. U. S. A.*, 2001, **98**, 8786–8791.
3 M. Lewin, N. Carlesso, C. H. Tung, X. W. Tang, D. Cory, D. T. Scadden and R. Weissleder, *Nat. Biotechnol.*, 2000, **18**, 410–414.
4 T. Schroder, K. Schmitz, N. Niemeier, T. S. Balaban, H. F. Krug, U. Schepers and S. Bräse, *Bioconjugate Chem.*, 2007, **18**, 342–354.
5 K. Eggenberger, E. Birtalan, T. Schroder, S. Bräse and P. Nick, *ChemBioChem*, 2009, **10**, 2504–2512.
6 P. A. Wender, D. J. Mitchell, K. Pattabiraman, E. T. Pelkey, L. Steinman and J. B. Rothbard, *Proc. Natl. Acad. Sci. U. S. A.*, 2000, **97**, 13003–13008.
7 C. Foged, H. Franzyk, S. Bahrami, S. Frokjaer, J. W. Jaroszewski, H. M. Nielsen and C. A. Olsen, *Biochim. Biophys. Acta*, 2008, **1778**, 2487–2495.
8 S. A. Fowler and H. E. Blackwell, *Org. Biomol. Chem.*, 2009, **7**, 1508–1524.
9 P. Armand, K. Kirshenbaum, R. A. Goldsmith, S. Farr-Jones, A. E. Barron, K. T. Truong, K. A. Dill, D. F. Mierke, F. E. Cohen, R. N. Zuckermann and E. K. Bradley, *Proc. Natl. Acad. Sci. U. S. A.*, 1998, **95**, 4309–4314.
10 C. W. Wu, K. Kirshenbaum, T. J. Sanborn, J. A. Patch, K. Huang, K. A. Dill, R. N. Zuckermann and A. E. Barron, *J. Am. Chem. Soc.*, 2003, **125**, 13525–13530.
11 S. B. Shin and K. Kirshenbaum, *Org. Lett.*, 2007, **9**, 5003–5006.
12 J. K. Pokorski, L. M. Jenkins, H. Feng, S. R. Durell, Y. Bai and D. H. Appella, *Org. Lett.*, 2007, **9**, 2381–2383.
13 B. C. Gorske, B. L. Bastian, G. D. Geske and H. E. Blackwell, *J. Am. Chem. Soc.*, 2007, **129**, 8928–8929.
14 K. Moehle and H. J. Hofmann, *Biopolymers*, 1996, **38**, 781–790.
15 K. Mohle and H. J. Hofmann, *J. Mol. Model.*, 1996, **2**, 307–311.
16 K. Kirshenbaum, A. E. Barron, R. A. Goldsmith, P. Armand, E. K. Bradley, K. T. Truong, K. A. Dill, F. E. Cohen and R. N. Zuckermann, *Proc. Natl. Acad. Sci. U. S. A.*, 1998, **95**, 4303–4308.
17 N. H. Shah, G. L. Butterfoss, K. Nguyen, B. Yoo, R. Bonneau, D. L. Rabenstein and K. Kirshenbaum, *J. Am. Chem. Soc.*, 2008, **130**, 16622–16632.
18 J. R. Stringer, J. A. Crapster, I. A. Guzei and H. E. Blackwell, *J. Am. Chem. Soc.*, 2011, **133**, 15559–15567.
19 P. A. Jordan, B. Paul, G. L. Butterfoss, P. D. Renfrew, R. Bonneau and K. Kirshenbaum, *Biopolymers*, 2011, **96**, 617–626.
20 P. Armand, K. Kirshenbaum, A. Falicov, R. L. Dunbrack Jr., K. A. Dill, R. N. Zuckermann and F. E. Cohen, *Folding Des.*, 1997, **2**, 369–375.
21 Q. Sui, D. Borchardt and D. L. Rabenstein, *J. Am. Chem. Soc.*, 2007, **129**, 12042–12048.
22 J. A. Crapster, J. R. Stringer, I. A. Guzei and H. E. Blackwell, *Biopolymers*, 2011, **96**, 604–616.
23 F. S. Nandel and A. Saini, *Macromol. Theory Simul.*, 2007, **16**, 295–303.
24 E. Birtalan, B. Rudat, D. K. Kolmel, D. Fritz, S. B. Vollrath, U. Schepers and S. Bräse, *Biopolymers*, 2011, **96**, 694–701.
25 U. Sternberg, F. T. Koch, M. Brauer, M. Kunert and E. Anders, *J. Mol. Model.*, 2001, **7**, 54–64.
26 R. Witter, L. Seyfart, G. Greiner, S. Reissmann, J. Weston, E. Anders and U. Sternberg, *J. Biomol. NMR*, 2002, **24**, 277–289.
27 M. Magzoub, L. E. Eriksson and A. Graslund, *Biochim. Biophys. Acta*, 2002, **1563**, 53–63.
28 A. Walrant, I. Correia, C. Y. Jiao, O. Lequin, E. H. Bent, N. Goasdoue, C. Lacombe, G. Chassaing, S. Sagan and I. D. Alves, *Biochim. Biophys. Acta*, 2011, **1808**, 382–393.
29 S. Deshayes, K. Konate, G. Aldrian, L. Crombez, F. Heitz and G. Divita, *Biochim. Biophys. Acta*, 2010, **1798**, 2304–2314.

30 P. Ruzza, A. Calderan, A. Guiotto, A. Osler and G. Borin, *J. Pept. Sci.*, 2004, **10**, 423–426.
31 A. Cavalli, X. Salvatella, C. M. Dobson and M. Vendruscolo, *Proc. Natl. Acad. Sci. U. S. A.*, 2007, **104**, 9615–9620.
32 Y. Shen, O. Lange, F. Delaglio, P. Rossi, J. M. Aramini, G. Liu, A. Eletsky, Y. Wu, K. K. Singarapu, A. Lemak, A. Ignatchenko, C. H. Arrowsmith, T. Szyperski, G. T. Montelione, D. Baker and A. Bax, *Proc. Natl. Acad. Sci. U. S. A.*, 2008, **105**, 4685–4690.
33 D. S. Wishart, D. Arndt, M. Berjanskii, P. Tang, J. Zhou and G. Lin, *Nucleic Acids Res.*, 2008, **36**, W496–W502.
34 U. Sternberg and M. Möllhoff, *J. Mol. Model.*, 2001, **7**, 90–102.
35 R. Witter, W. Priess and U. Sternberg, *J. Comput. Chem.*, 2002, **23**, 298–305.
36 U. Sternberg, *Mol. Phys.*, 1988, 63.
37 W. Kutzelnigg, *Isr. J. Chem.*, 1980, **19**, 193.
38 I. Jakovkin, M. Klipfel, C. Muhle-Goll, A. S. Ulrich, B. Luy and U. Sternberg, *Phys. Chem. Chem. Phys.*, 2012, **14**, 12263–12276.
39 U. Sternberg, A. S. Ulrich and R. Witter, *Annu. Rep. NMR Spectrosc.*, 2004, **52**, 53–104.